

## Water Chemistry Impacts on Arsenic Mobilization from Arsenopyrite Dissolution and Secondary Mineral Precipitation: Implications for Managed Aquifer Recharge

Chelsea W. Neil,<sup>†</sup> Y. Jeffrey Yang,<sup>‡</sup> Don Schupp,<sup>§</sup> and Young-Shin Jun<sup>\*,†</sup>

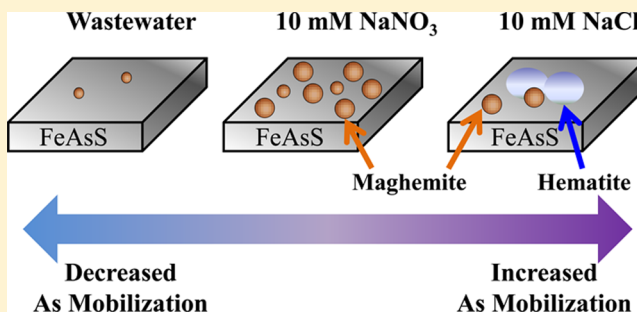
<sup>†</sup>Department of Energy, Environmental and Chemical Engineering, Washington University, St. Louis, Missouri 63130, United States

<sup>‡</sup>Office of Research and Development, National Risk Management Research Laboratory, U.S. Environmental Protection Agency, Cincinnati, Ohio 45268, United States

<sup>§</sup>CB&I, 5050 Section Avenue, Cincinnati, Ohio 45212, United States

### Supporting Information

**ABSTRACT:** Managed aquifer recharge (MAR) is a water reuse technique with the potential to meet growing water demands. However, MAR sites have encountered arsenic mobilization resulting from recharge operations. To combat this challenge, it is imperative to identify the mechanisms of arsenic mobilization during MAR. In this bench-scale study, arsenic mobilization from arsenopyrite (FeAsS) was characterized for conditions relevant to MAR operations. Experimentally determined activation energies for arsenic mobilization from FeAsS under aerobic conditions were  $36.9 \pm 2.3$  kJ/mol for 10 mM sodium chloride,  $40.8 \pm 3.5$  kJ/mol for 10 mM sodium nitrate, and  $43.6 \pm 5.0$  kJ/mol for secondary effluent from a wastewater treatment plant. Interestingly, the sodium chloride system showed higher arsenic mobilization under aerobic conditions. In addition, secondary mineral precipitation varied among systems and further affected arsenic mobilization. For example, the wastewater system inhibited precipitation, while in the sodium chloride system, faster phase transformation of iron(III) (hydr)oxide precipitates was observed, resulting in hematite formation after 7 days. The phase transformation to hematite will result in less available surface area for arsenic attenuation. These new observations and activation energies can be useful to develop improved reactive transport models for the fate of arsenic during MAR, and develop strategies to minimize arsenic release.



### INTRODUCTION

Increasing groundwater demands have resulted in widespread depletion of aquifers—the underground formations that store 98% of the world's fresh water resources.<sup>1</sup> In addition to drinking and sanitation water shortages, lowered groundwater tables can lead to the drying of wetlands, destructive settling of surrounding lands, and contamination of groundwater by saltwater intrusion.<sup>2–4</sup> Natural recharge rates will depend on climate, soil composition, and aquifer depth, and can vary significantly in space and time. Groundwater overdrafting also occurs when withdrawal exceeds these natural recharge rates. Therefore, it is vital to establish a safe and sustainable means of supplementing natural groundwater recharge to avoid undesired detrimental health and environmental impacts.

Managed aquifer recharge (MAR) is considered to be a water reuse solution to address water needs in areas where water demand exceeds the natural recharge potential.<sup>5–7</sup> MAR operations involve the injection and storage of secondary water into subsurface strata, including groundwater aquifers, for future use. Recharge water can be utilized from a variety of natural sources including available surface waters, stormwater runoff, and snowmelt.<sup>5</sup> In addition, one common source for the

secondary water utilized in MAR is “reclaimed” wastewater, which has been treated beyond conventional wastewater treatment.<sup>8–10</sup> Natural attenuation processes in the vadose zone and underlying aquifer have been shown to remove residual pathogens from the injected secondary water.<sup>11,12</sup> However, recent studies at MAR field sites have shown that reclaimed water recharge can trigger unfavorable soil–water interactions releasing arsenic, a toxic metalloid, from aquifer materials. For example, Jones and Pichler<sup>13</sup> reported that while injection waters to a MAR site in South Central Florida contained 3 µg/L of arsenic, recovered levels were much higher, ranging from 10 to 130 µg/L. Arsenic mobilization as a result of artificial aquifer recharge has also been observed globally at sites in Australia, Germany, China, and The Netherlands, as well as in states in the USA, including Florida, California, Wisconsin, Idaho, and Montana.<sup>14</sup> Some of these locations, such as Bolivar, South Australia<sup>10</sup> and Manatee, FL<sup>15</sup>

Received: November 17, 2013

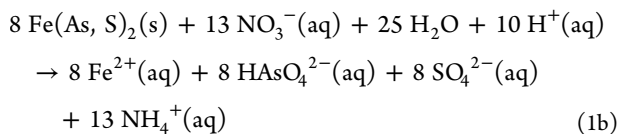
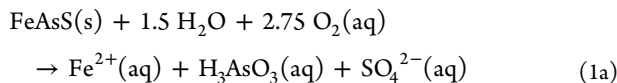
Revised: March 7, 2014

Accepted: March 12, 2014

Published: March 12, 2014

reported initial low ambient arsenic concentration of 3 and 8 µg/L, respectively. MAR implementation at these sites led to recovered levels of 22.5 and 24 µg/L. Instances of arsenic mobilization from Suwannee Limestone during MAR in Florida stemmed from arsenian pyrite containing arsenic at levels of up to 1.12 wt % arsenic.<sup>16</sup> In many of these instances, recovered arsenic levels have exceeded the Environmental Protection Agency's maximum concentration level of arsenic, which is 10 µg/L. Therefore, the risk for arsenic mobilization during MAR can be widespread, and a better understanding of the effects of water chemistry of the injected water on arsenic mobilization is needed.

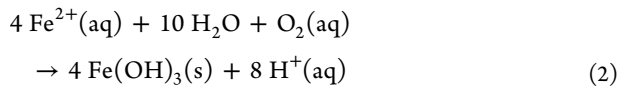
Despite many observations and intense studies in multiple aquifer systems,<sup>10,13–15</sup> consensus has not been reached on the dominant cause of this observed arsenic mobilization. One proposed mechanism is the oxidation of arsenic-bearing minerals, such as arsenopyrite (FeAsS) or arsenian pyrite (< 0.5–10 wt % As),<sup>17</sup> by the electron acceptors oxygen and/or nitrate (eq 1a–b), which may not be otherwise present in anoxic native groundwater:<sup>13,14,18,19</sup>



Dissolution products can be further oxidized from Fe(II) to Fe(III) and As(III) to As(V).

The existence of arsenopyrite and arsenic-bearing pyrite in groundwater aquifers is documented frequently, as is its effect on groundwater arsenic levels.<sup>16,20–22</sup> The oxidation of arsenic-bearing pyrite in sandstone drinking water aquifers in Northeastern Wisconsin has led to arsenic levels exceeding 50 µg/L in 86 of 2125 water supply wells.<sup>20</sup> Arsenopyrite found in bedrock in south-central New Hampshire was responsible for elevated arsenic in domestic wells of up to 180 µg/L.<sup>21</sup> Furthermore, MAR would not be solely utilized to replenish drinking water supplies. Groundwater demands must also be met for irrigation and industrial uses, and overdraining is an issue in many deeper aquifers used for this purpose. High levels of naturally occurring arsenic have also been found in these deeper groundwater aquifers. For example, arsenic concentrations of 1–10 mg/L have been observed in groundwater in Fairbanks, Alaska, due to the presence of arsenopyrite-rich sediments.<sup>22</sup> In addition, recent aquifer storage activities have involved bedrock aquifers of metamorphic or igneous origins, which are more likely to contain arsenopyrite or arsenian pyrite. These activities include surface water replenishment programs and energy-exploration water disposal in such areas as Colorado, Utah, and further northwest in the U.S.<sup>23,24</sup>

Furthermore, arsenic mobilization in groundwater will be governed in part by interactions with iron(III) (hydr)oxide minerals, which have a large capacity for sorbing aqueous arsenic. Iron(III) (hydr)oxides (Fe(OH)<sub>3</sub>; simplified form of ferrihydrite) can form in aqueous environments and as a product of arsenopyrite oxidation:<sup>25,26</sup>



Although many studies exist on groundwater–arsenic-bearing pyrite interactions<sup>27,28</sup> and the subsequent fate and transport of arsenic in groundwater,<sup>29,30</sup> no study to date has fully addressed the unique scenario of MAR using reclaimed wastewater. This is in part due to the complicated nature of this scenario, as wastewater not only has many constituents, but also its composition will not be constant during MAR operations or between different MAR sites. We must, therefore, systematically characterize the potential interactions between prevailing reclaimed water components and arsenic-bearing pyrite to establish best practices for MAR and increase its viability as a water reuse option. To achieve this, we start the investigation with model systems, where water chemistry and solid phase composition are controlled to identify dominant arsenic mobilization mechanisms, as well as furthering our understanding of wastewater–arsenic-bearing pyrite interactions. Arsenopyrite was chosen as the model arsenic-bearing pyrite for these systems in order to guarantee that samples utilized in different solution and solid-phase experiments have uniform compositions, allowing us to quantify mobilization and precipitation, and systematically compare results among different systems. Outcomes from these well-characterized, model studies will also provide a baseline for future studies utilizing arsenian pyrite and field site samples.

This bench-scale study, therefore, aims to examine the kinetics of arsenic mobilization from arsenopyrite in the presence of reclaimed wastewater and two model wastewater solutions of simplified composition containing either sodium chloride or sodium nitrate at comparable ionic strengths to reclaimed water. These different anions were chosen to study because of their presence in reclaimed wastewater and their known impact on the formation of ferrihydrite, a secondary mineral product of arsenopyrite dissolution.<sup>26</sup> Changes in the arsenopyrite solid phase were also examined to determine the extent and phase of secondary mineral precipitation. This is important because arsenopyrite oxidation during MAR operations has been reported to form iron(III) (hydr)oxide minerals such as ferrihydrite, which can impact aqueous arsenic levels by immobilizing arsenic through sorption and coprecipitation. For this work, we focused on the inorganic water components that can influence arsenic mobilization during MAR. The new quantitative and qualitative information gained in this study will improve current reactive transport models for arsenic fate and transport analysis during MAR. Moreover, the new knowledge acquired can be applied to other systems where arsenic pollution of groundwater is a concern, such as acid mine drainage sites,<sup>30</sup> uranium mine tailing operations,<sup>31,32</sup> and locations with pervasive natural arsenic contamination.<sup>33,34</sup>

## EXPERIMENTAL SECTION

**Aqueous Phase Characterization in Batch Reactor Experiments.** *Solid and Solution Sample Preparation.* For all experiments, natural arsenopyrite samples were used. Arsenopyrite samples from Gold Hill, Tooele County, UT, were purchased from the Mineralogical Research Company (San Jose, CA). X-ray diffraction (XRD), scanning electron microscopy with energy-dispersive X-ray spectroscopy (SEM-EDX), and Raman spectroscopy all confirmed that these samples contained a mixture of quartz and arsenopyrite (Figure S1A in the Supporting Information (SI)). Raman spectroscopy produced two different characteristic spectra depending on whether the beam was focused on quartz or arsenopyrite in the sample powder (SI Figure S1B). These were compared with the

literature and identified as arsenopyrite and quartz.<sup>35,36</sup> Arsenopyrite ore samples were ground using a mortar and pestle to produce an array of particle sizes that were separated using sieves. For batch reactor dissolution experiments, 300–500 μm particles were used. The surface area of the 300–500 μm particles was determined using Brunauer–Emmett–Teller (BET) to be 0.116–0.555 m<sup>2</sup>/g from three measurement trials. Although there is a high variability in surface area measurements, experiments were conducted using the same arsenopyrite mass and particle size range, while the grain purity, texture, and quality was maintained. Therefore, the surface area for each system is expected to be similar. Due to the potential variability in surface area measurements, surface area was not used to normalize dissolution rates. Because arsenopyrite may be oxidized when being exposed to atmospheric oxygen, powdered samples were cleaned using an acid-washing procedure established by McGuire et al. and stored in an anaerobic chamber prior to reaction.<sup>37</sup>

Solutions containing 10 mM sodium nitrate or 10 mM sodium chloride were created using reagent-grade salts. The pH of these solutions was adjusted prior to reaction to  $7.0 \pm 0.2$  using nitric acid for the sodium nitrate solution or hydrochloric acid for the sodium chloride solution. The pH was chosen to match the pH of wastewater samples, which ranged from 6 to 8, and an ionic strength of 10 mM was chosen to match the conductivity of the wastewater samples ( $\sim 1100 \mu\text{S}/\text{cm}$ ). Conductivity was measured using an Orion DuraProbe conductivity cell (Thermo Scientific, MA) and pH was measured using a pH electrode (Mettler-Toledo, OH). Conductivity and pH values did not vary significantly among five reclaimed wastewater samples taken at different times from the Cincinnati treatment facility. Concentrations of nitrate reported in the literature for tertiary effluent range from 0.52 to 1.16 mM.<sup>38–41</sup> Although the nitrate concentration used in this study is higher than reported values, to help delineate the effects of chloride on secondary mineral precipitation, 10 mM nitrate was chosen to be the same as the chloride concentration. Nitrate can provide valuable data for comparison with sodium chloride because nitrate does not form significant complexation with aqueous Fe(III) as chloride does.

During the 6-h reaction period, the pH of the sodium nitrate and sodium chloride systems decreased to 6.3 and 6.8, respectively, while the pH of the wastewater system increased to 7.7. Wastewater used for the experiments was secondary effluent obtained from the Metropolitan Sewer District of Greater Cincinnati (MSDC) wastewater treatment plant (samples were collected in November 2012).

Table 1 shows the aqueous composition of the wastewater used in the experiments. The concentration of metal ions in the wastewater was measured using inductively coupled plasma-mass spectrometry (ICP-MS) (7500ce, Agilent Technologies, CA); the concentration of chloride was measured using a chloride ion selective probe (VWR International Inc., West Chester, PA); and the nonpurgeable total organic carbon (TOC) content was determined using a Shimadzu TOC-LCPH analyzer. Prior to reaction, the pH of the wastewater was adjusted to  $7.0 \pm 0.2$  using nitric acid. For anaerobic systems, pH 7, 10 mM sodium nitrate or sodium chloride solutions were made in an anaerobic chamber using deoxygenated water ( $P_{\text{O}_2} = 0 \text{ atm}$ ). Wastewater samples were deoxygenated by stirring them for at least 48 h in the anaerobic chamber. Anoxic

**Table 1. Selected Principal Wastewater Constituents for Samples Provided by the Greater Cincinnati Metropolitan Sewer District Wastewater Treatment Plant in November 2012<sup>a</sup>**

constituent	concentration
lithium	0.547 μM
sodium	188.2 μM
magnesium	78.17 μM
aluminum	0.074 μM
potassium	9.97 μM
calcium	67.5 μM
manganese	0.180 μM
iron	1.31 μM
nickel	0.025 μM
copper	0.005 μM
zinc	0.024 μM
arsenic	0.003 μM
chloride	6.27 mM
pH	7.3
TOC	12.42 mg/L

<sup>a</sup> Metal ion concentrations were determined by ICP-MS, chloride ion concentrations were determined using a chloride ion selective electrode, and total organic carbon was measured using a TOC analyzer

conditions were confirmed using a dissolved oxygen (DO) probe and oxygen gas analyzer in the anaerobic chamber.

**Batch Reactor Experimental Approach.** Batch reactors were used to determine dissolution rates for arsenopyrite under different experimental conditions. Zero-order reaction kinetics were confirmed by the linear concentration evolution of arsenic in the reactor (trend lines in Figure 1). Each batch reactor contained 250 mL of the reaction solution and 0.05 g of acid-washed FeAsS powder. Reactors were continuously stirred, and the temperature was controlled at 5, 22, or  $35 \pm 1^\circ\text{C}$  using a hot water or ice bath. A 2 mL sample was removed at 0, 0.5, 1, 2, 3, 4, 5, and 6 h and filtered immediately using a 0.2-μm polytetrafluoroethylene (PTFE) membrane syringe filter and capped to prevent evaporative losses. This time frame was chosen to minimize the effect of secondary mineral precipitation on aqueous arsenic levels. Finally, samples were acidified to 2% v/v acid, and arsenic concentrations were measured using ICP-MS. At least three experimental replicates were run to confirm arsenic mobilization trends.

During investigation of secondary mineral precipitation on arsenopyrite, batch reactors were run for the longer time frame of 7 days (a detailed description in the next sections). For these experiments, arsenic speciation in solution samples reacted for 1 and 7 days was carried out using an anion-exchange column packed with Spectra/Gel Ion exchange resin in its chloride form (Spectrum Laboratories, CA).<sup>42</sup> First, 10 mL of filtered batch reactor supernatant was adjusted to pH 3.5. The solution was then passed through the column where the first 5 mL was discarded and the next 5 mL was collected for analysis. Using this method, As(V) was retained in the columns while As(III) passed through the column. Comparison of As levels measured using ICP-MS in the influent and effluent was used to determine quantities of As(III) and As(V).

**Characterization of Secondary Mineral Precipitate Morphology and Mineralogy.** *Substrate Sample Preparation.* Morphological changes on the arsenopyrite mineral surface were examined using polished 1 mm-thin arsenopyrite

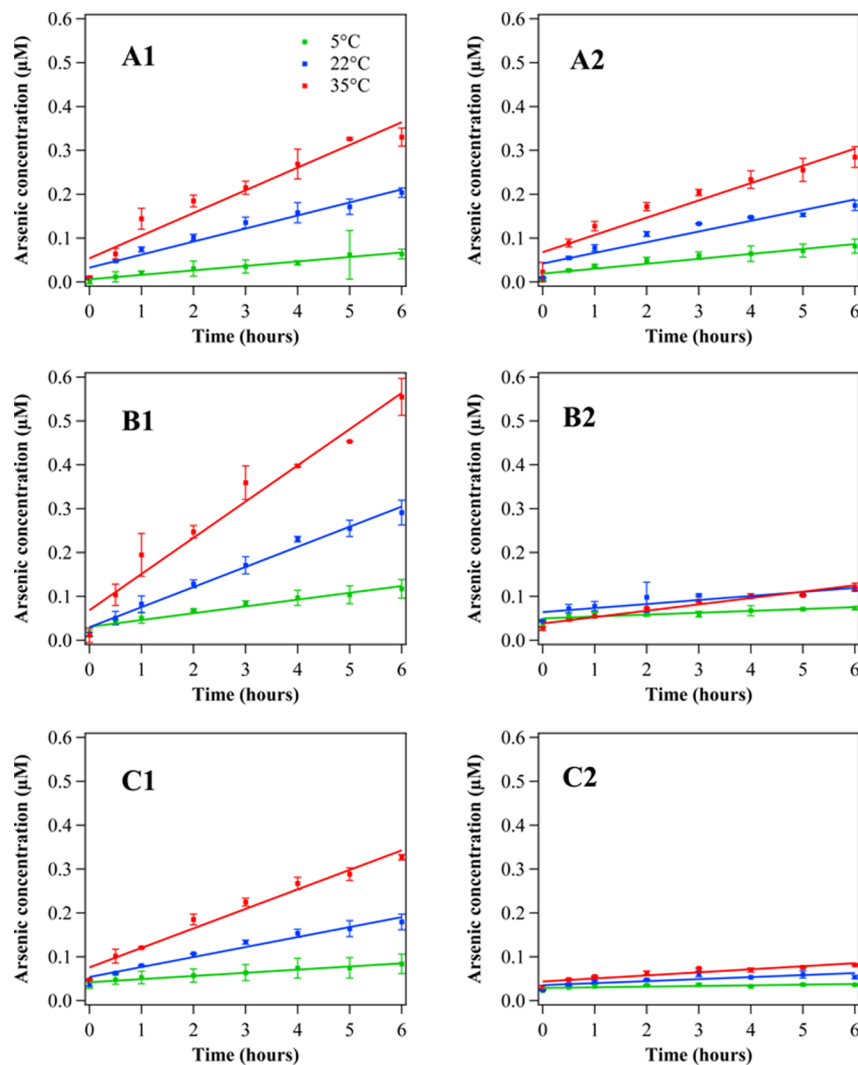


**Figure 1.** Aqueous arsenic concentration evolutions in batch reactors at 5, 22, and 35 °C over the 6-h reaction period for (A1) pH 7, 10 mM sodium nitrate, aerobic, (A2) pH 7, 10 mM sodium nitrate, anaerobic; (B1) pH 7 10 mM sodium chloride, aerobic, (B2) pH 7, 10 mM sodium chloride, anaerobic; and (C1) pH 7 wastewater, aerobic, (C2) pH 7 wastewater, anaerobic. Standard deviations between replicate trials are indicated by error bars.

sections, called “coupons”. Samples were mounted on glass slides using an acetone-soluble epoxy, which was removed before coupons were used in experiments. A uniformly flat surface was confirmed for unreacted arsenopyrite coupons using atomic force microscopy (AFM) (SI Figure S2) and coupons were stored in the anaerobic chamber. Coupons were cleaned immediately prior to reaction using acetone, ethanol, and isopropanol to remove any organic coating, and rinsed with deionized water. Solutions used for solid characterization experiments were created identically to aqueous phase experiments.

**Instrumental Analyses of Precipitates.** To observe the effects of water chemistry on the extent and morphology of secondary mineral precipitation, coupons were reacted under the same conditions used for aqueous-phase experiments. Multiple small coupons were added to batch reactors containing 250 mL of solution and 0.05 g of arsenopyrite at room temperature (22 °C). Samples were removed after 6 h, 1 day, 4 days, and 7 days, rinsed with deionized water, and dried with high purity nitrogen gas. The longer time frame allowed better observation of secondary mineral formation and phase

transformation, which could potentially occur at MAR sites where groundwater flow is near-stagnant. To prevent further oxidation, reacted coupons were stored in the anaerobic chamber prior to and after analysis using AFM and Raman spectroscopy.

Tapping mode AFM (AFM, Veeco Inc.) was used to characterize secondary mineral precipitates on arsenopyrite coupons by measuring changes in the height, amplitude, and phase over the 7-day reaction period. AFM tapping mode probes were 125 μm long with phosphorus (n) doped silicon tips (nominal tip radius of 10 nm, MPP-11100-10, Bruker probes). A scanning rate of 0.988 Hz and drive frequencies between 312 and 320 kHz were used during imaging. To obtain better statistical information and confirm observed precipitation trends, each sample was measured at multiple locations on the substrate surface using different scan sizes. Images were processed using Nanoscope 7.20 software.

Raman spectroscopy was conducted using an inVia Raman Microscope (Renishaw, UK) on reacted arsenopyrite in order to identify secondary mineral precipitates. Raman measurements were carried out with a 514 nm laser and a grating of

1800 lines/mm. A 20 $\times$  objective and decreased power were used to limit the energy density of the laser, preventing artificial phase transformation of secondary mineral precipitates.<sup>43</sup> Raman analysis was also conducted using the same instrument on a number of iron oxides standards and unreacted arsenopyrite in order to identify their characteristic peaks for comparison with reacted samples.

## RESULTS AND DISCUSSION

**Water Chemistry. Evolution of Aqueous Arsenic Concentration.** Figure 1 shows the arsenic concentration changes with time in the aqueous phase for 10 mM sodium nitrate, 10 mM sodium chloride, and wastewater under aerobic (A1, B1, and C1) and anaerobic (A2, B2, and C2) conditions. Among aerobic systems, the highest arsenic mobility was observed in the 10 mM sodium chloride system. Arsenic concentrations were similar between the wastewater and sodium nitrate systems. The only difference between the two model wastewater systems was the presence of nitrate versus chloride anions, neither of which are expected to interact significantly with arsenopyrite in the presence of dissolved oxygen according to the literature.<sup>44</sup> In addition, neither nitrate nor chloride competes with arsenate for Fe(III) adsorption sites.<sup>45–47</sup> Therefore, differences in the arsenic mobility are not anticipated to result from changes in the oxidative dissolution of arsenopyrite or sorption of arsenic, but, more likely, from effects on secondary mineral formation and phase transformation, which further impact arsenic attenuation.

For the anaerobic system, the highest arsenic concentration was observed in the sodium nitrate system (up to 0.28 mM), while very low concentrations were observed in the 10 mM sodium chloride and wastewater systems (up to 0.12 and 0.08 mM, respectively). For all systems, arsenic mobility was lower under anaerobic conditions (15%, 78%, and 76% reductions for nitrate, chloride, and wastewater systems, respectively, compared to aerobic conditions based on the 6-h time frame), indicating the role of dissolved oxygen in the oxidative release of arsenic from arsenopyrite through reaction eq 1a. The decreased percent reduction in the anaerobic 10 mM sodium nitrate system compared to wastewater and sodium chloride can be due to the oxidation of arsenopyrite by nitrate anions in the absence of dissolved oxygen.<sup>48–50</sup>

**Activation Energy Calculations.** For all aqueous systems, the activation energies for arsenic mobilization were calculated using the Arrhenius equation. Because zero-order reaction kinetics were observed in the early stages of dissolution, the slope of the concentration evolution at each temperature (e.g., trend lines in Figure 1) was assumed to be equal to the rate constant,  $k$ , of the reaction. A larger rate constant would therefore correlate with higher arsenic concentrations at the end of the 6-h reaction period. The rate constant,  $k$ , is related to the temperature and activation energy in accordance with the Arrhenius equation:

$$k = Ae^{-E_a/RT} \quad (3)$$

Taking the natural logarithm of this equation gives a linear relationship between the rate constant and temperature,  $T$ :

$$\ln(k) = \frac{-E_a}{R} \frac{1}{T} + \ln(A) \quad (4)$$

The rate constant  $k$  for each reaction condition was determined by calculating the slope of the best fit trend line for the concentration evolution at each temperature. The natural log of

$k$  was plotted against the inverse of the temperature and the slope of this line was equal to the negative activation energy,  $E_a$ , divided by the gas constant,  $R$ . For the aerobic systems, the calculated activation energies for arsenic mobilization were  $40.8 \pm 3.5$ ,  $36.9 \pm 2.3$ , and  $43.6 \pm 5.0$  kJ/mol for 10 mM sodium nitrate, 10 mM sodium chloride, and wastewater, respectively. For the anaerobic systems, the calculated activation energies for arsenic mobilization were  $31.2 \pm 3.2$ ,  $28.4 \pm 3.6$ , and  $44.1 \pm 6.3$  kJ/mol for 10 mM sodium nitrate, 10 mM sodium chloride, and wastewater, respectively (Table 2). The activation energies

**Table 2. Empirically Determined Activation Energies for Arsenic Mobilization from Arsenopyrite<sup>a</sup>**

aqueous media	temperatures (°C)	activation energies (kJ/mol) <sup>b</sup>	
		aerobic	anaerobic
10 mM sodium nitrate	5, 22, and 35	$40.8 \pm 3.5$	$31.2 \pm 3.2$
10 mM sodium chloride	5, 22, and 35	$36.9 \pm 2.3$	$28.4 \pm 3.6$
wastewater	5, 22, and 35	$43.6 \pm 5.0$	$44.1 \pm 6.3$

<sup>a</sup>All reactions were carried out at pH  $7.0 \pm 0.2$ . The solid-to-liquid ratio was 250 mL:0.05 g FeAsS powder. The surface area of FeAsS coupons added during the experiments was calculated and found to be negligible compared to the area of the FeAsS powder. Triplicate reactors were run for all temperatures. <sup>b</sup>Standard error for  $E_a$  values was determined using the following equation:  $SE = ((1/(n - 2))\sum_{i=1}^n(y - \hat{y})^2)/\sum_{i=1}^n(x - \bar{x})^2)^{1/2}$

for iron release were not calculated because aqueous iron levels were below the detection limit during the 6-h reaction period. This may result from the reprecipitation of aqueous iron as iron(III) (hydr)oxides. We expect that this process will further impact aqueous arsenic levels through concurrent arsenic sorption or coprecipitation. Therefore, while activation energies for arsenic mobilization would not be equivalent to that of arsenopyrite oxidation, it provides a better indicator of the overall arsenic mobility in these systems.

The literature provides activation energies for a number of minerals related to this system, including the oxidation of arsenopyrite by dissolved oxygen (57 kJ/mol at pH 5.9),<sup>51</sup> and the reductive dissolution of ferrihydrite (40.7 kJ/mol),<sup>52</sup> hematite (88 kJ/mol),<sup>53</sup> and goethite (94 kJ/mol).<sup>53</sup> The range of observed activation energies indicates that the most likely processes occurring are the oxidation of arsenopyrite by dissolved oxygen or the reduction of ferrihydrite, because all measured activation energies ranged between 30 and 50 kJ/mol. However, our numbers are slightly different from the literature as we are focused on the overall arsenic mobility, i.e., the balance between arsenic release and attenuation, in MAR-related systems. Interestingly, for the wastewater systems, the activation energy did not change between the aerobic and anaerobic systems. Despite the lower activation energy for 10 mM sodium nitrate and 10 mM sodium chloride in anaerobic systems, the mobility of arsenic was 3.5 times higher in nitrate and 1.5 times higher in chloride compared to the wastewater system. This indicates that other factors, such as the availability of reactants, contributed to decrease arsenic mobilization. To investigate these observed trends and to determine secondary mineral effects on aqueous arsenic mobilization, the differences in secondary mineral formation and phase transformation among sodium nitrate, sodium chloride, and wastewater systems were studied.

**Characterization of Secondary Mineral Precipitate Morphology and Mineralogy.** *Secondary Mineral Morphology and Coverage.* Differences in secondary mineral precipitation among the three aqueous systems yield further insight into the observed trends in arsenic mobilization. Figure 2 shows the AFM height mode images after 1 day and 7 days in

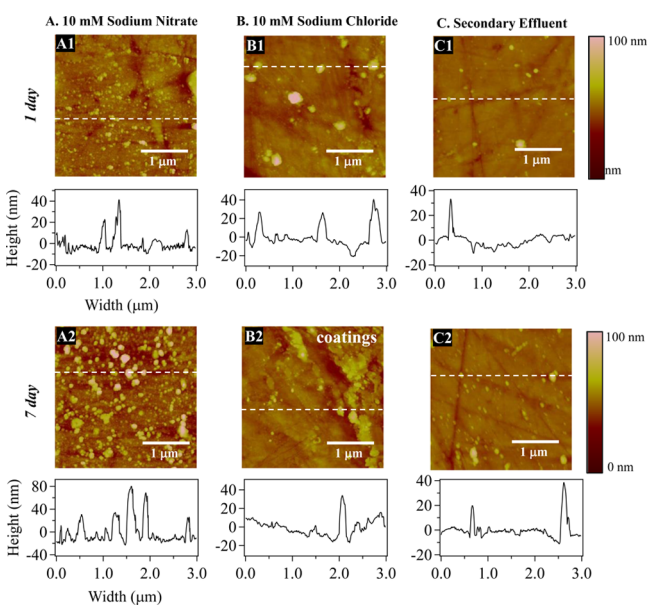


**Figure 2.** AFM height mode images after 1 day (A1, B1, and C1) and 7 days (A2, B2, and C2) in the 10 mM sodium chloride, 10 mM sodium nitrate, and wastewater systems, respectively at room temperature (22 °C) and under aerobic conditions. Dotted lines indicate where the image was cut to produce the height profile graphs below each image. The scan size for these images is 3 μm and the height scale is 100 nm. Images of the unreacted coupon can be found in SI Figure S3.

the 10 mM sodium chloride, 10 mM sodium nitrate, and wastewater systems at room temperature (22 °C) and under aerobic conditions. Images at additional time points are provided in SI Figure S3. For all time points, multiple images were taken over the entire sample surface to confirm observations. The images in Figure 2 showed very distinct differences in precipitate morphology between the three systems. For the 10 mM sodium nitrate system, after 1 day there was a significant amount of small precipitates covering the entire surface (Figure 2A1). After 7 days, these precipitates grew in quantity and size, and at the end of the reaction period there was a variety of both large and small particles, indicating continued nucleation and growth for the entire period (Figure 2A2). For the 10 mM sodium chloride system (Figure 2B), particles after 1 day were larger in size and sparse on the surface. After 7 days, these particles appeared to aggregate to form a continuous coating on the surface. Unlike the sodium nitrate system, there was not much evidence of continued nucleation because the size and morphology of precipitates was very different between days 1 and 7. For the wastewater system (Figure 2C), there was little precipitation after 1 day and both the size and morphology of precipitates did not change significantly over 7 days. Under anaerobic conditions, there was no observed precipitation on the coupons for all three systems even after 7 days (SI Figure S4).

**Secondary Mineral Phase Identification.** Identification of secondary mineral phases in aerobic systems was accomplished using Raman spectroscopy. The characteristic spectra for different iron oxide minerals were determined by measuring standard samples on the Raman instrument. For the anaerobic system, there was no precipitation detectable by Raman spectroscopy and AFM (SI Figure S4).

Early in the reaction period (< 1 day), there was no detectable secondary mineral precipitation on the surface for any system. In the sodium nitrate system, the characteristic peaks of maghemite ( $\gamma\text{-Fe}_2\text{O}_3$ ), an iron(III) oxide polymorph, become detectable after 1 day of reaction (Figure 3B). By 7 days, the entire coupon surface in the sodium nitrate system was coated by maghemite (Figure 3A). For the sodium chloride system, no precipitation was detected after 1 day owing to the small quantity of precipitates. After 7 days, however, the surface was covered in a nonhomogeneous coating of hematite ( $\alpha\text{-Fe}_2\text{O}_3$ ) and maghemite (Figure 3D). The visual difference between these two mineral phases is apparent on the arsenopyrite surface (Figure 3C). For the wastewater system, there was no detectable precipitation even over the 7-day reaction period. Six-line ferrihydrite, magnetite, and goethite standards were also considered, but the spectra did not match the reacted samples.

**Mechanism of Secondary Mineral Phase Transformation in Nitrate and Chloride Systems.** In general, hematite is the most thermodynamically stable iron oxide polymorph and is the final form resulting from the transformation of less thermodynamically stable iron(III) (hydr)oxides.<sup>54</sup> The occurrence of hematite in the sodium chloride system and not the sodium nitrate system after 7-days reaction time was confirmed by multiple replicates. The faster transformation of iron(III) (hydr)oxides in the presence of sodium chloride compared to sodium nitrate is a new interesting observation, and can greatly impact arsenic mobilization from arsenopyrite.

Previous research conducted into the effects of chloride and nitrate on heterogeneous and homogeneous iron(III) (hydr)-oxide nucleation and growth provides insight into this phenomenon.<sup>55</sup> Using time-resolved small-angle X-ray scattering (SAXS) and grazing-incidence SAXS, Hu et al. observed that in the presence of chloride ions, Ostwald ripening was the dominant process controlling heterogeneous precipitation, whereas continuous nucleation, growth, and aggregation occurred in the nitrate system.<sup>55</sup> Ostwald ripening describes the growth mechanism wherein smaller precipitates dissolve and form larger and more thermodynamically stable precipitates on the surface, resulting in an increase in particle size while the total number of particles decreases. In other words, through Ostwald ripening the particles can undergo phase transformation from less stable iron(III) (hydr)oxide polymorphs such as ferrihydrite into more stable forms, such as maghemite and, eventually, hematite.<sup>56,57</sup>

The differences reported by Hu et al. in the iron(III) (hydr)oxide growth mechanisms are observable in AFM images of arsenopyrite coupons after 1 and 7 days reaction time (Figure 2). In the sodium nitrate system, small particles are always visible on the surface in addition to larger aggregates, indicating continued nucleation, growth, and aggregation. Based on size analyses of more than 100 particles, particle heights increased in the sodium nitrate system, from 10–30 nm after 1 day to 50–80 nm after 7 days. In the sodium chloride system, larger particles of around  $40 \pm 10$  nm with a smaller number of particles are visible after 1 day. This height did not

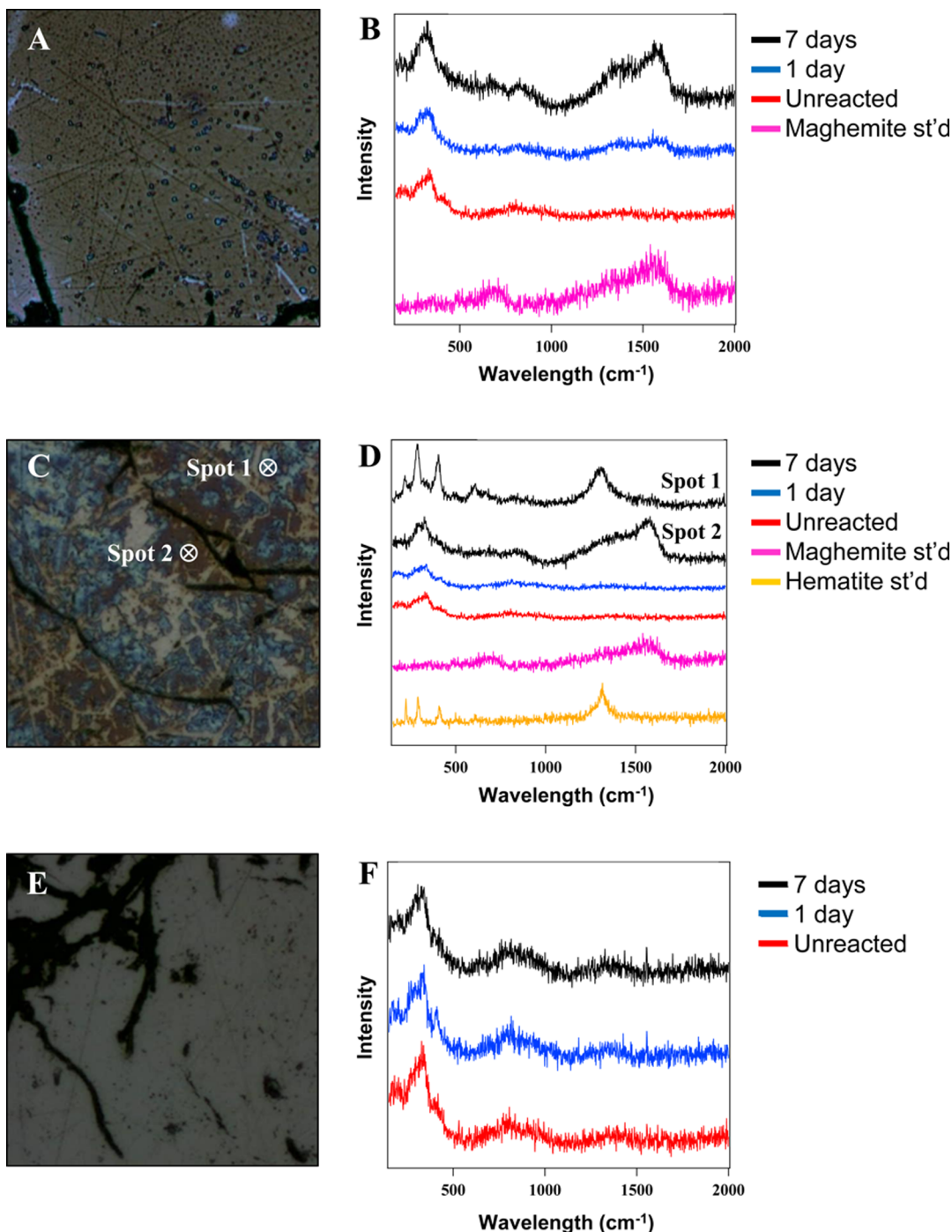


**Figure 3.** Optical microscope images and Raman spectra for arsenopyrite coupons reacted in sodium nitrate (A, B), sodium chloride (C, D), and wastewater (E, F) systems. Optical microscope images for the 7-day sodium nitrate system (A) shows a uniform coating of maghemite, as indicated by the characteristic Raman peaks (B). For the sodium chloride system, after 7 days, the surface was covered in a nonhomogeneous coating (C) of hematite ( $\alpha\text{-Fe}_2\text{O}_3$ ) and maghemite (D). No precipitation was observed in the wastewater system (E, F).

increase after 7 days, while lateral dimensions of particles increased greatly, forming a continuous iron(III) (hydr)oxide coating after 7 days (Figure 2B2). Furthermore, there is a lack of smaller precipitates in both the 1- and 7-day samples, indicating that primary particles may have gone through Ostwald ripening processes. The prevalence of Ostwald ripening as a growth mechanism can also explain the faster phase transformation observed in the sodium chloride system. In the presence of chloride, soluble ferric chloride complexes can form.<sup>58</sup> These complexes would decrease the apparent

saturation ratio with respect to iron(III) (hydr)oxides in the system. Due to the lower saturation ratio, it will be more thermodynamically favorable to form stable crystalline phases rather than metastable phases, which require larger saturations.<sup>59,60</sup> This phenomenon may explain why iron(III) (hydr)oxides in the sodium chloride system will form the more stable polymorph, hematite, within 7 days, while this phase is not present in the sodium nitrate system. However, additional mechanistic studies are needed to fully elucidate the role of chloride in this system.

The Ostwald ripening phenomenon will have secondary effects on arsenic mobility in the sodium nitrate and sodium chloride systems. Increased iron(III) (hydr)oxide nucleation in the sodium nitrate system leads to a large number of smaller particles. The high cumulative surface area of these precipitates can lead to more available surface sites for the sorption of aqueous arsenic anions, resulting in lower arsenic concentrations. Sorption quantities would also affect aqueous arsenic speciation. At pHs below 7, which were observed for 7-day batch reactor experiments (Figure 4), As(V) will sorb more

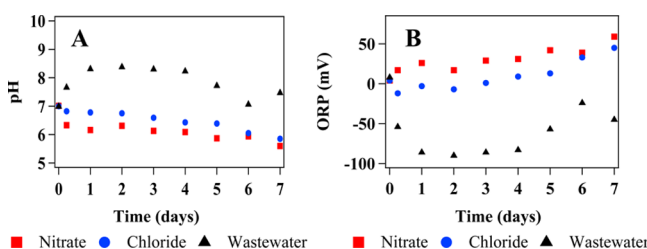


**Figure 4.** Evolutions of pH and ORP in aerobic batch reactors over the 7-day reaction period. The pH value was not adjusted over this time. All reactors were at room temperature (22 °C) and open to the atmosphere ( $P_{O_2} = 0.21$  atm).

readily to iron(III) (hydr)oxides.<sup>61</sup> Over the reaction period, the percentage of aqueous As(V) decreased for the sodium nitrate system from 62.7%As(V) (i.e., 37.3% As(III)) at 1 day to 53.1% at 7 days. The percentage of aqueous As(V) increased from 55.3% to 65.9% for sodium chloride and 59.3% to 77.1% for reclaimed water. These trends indicate that for the sodium nitrate system, aqueous As(III) was oxidized to As(V) and sorbed onto iron(III) (hydr)oxide precipitates, while for the sodium chloride system and reclaimed water system there was less capacity for As sorption compared to the sodium nitrate system. This would occur because the reclaimed water system had less precipitation compared to sodium nitrate system, and the sodium chloride had more crystalline precipitates (e.g., hematite). This mechanism is consistent with observations of enhanced arsenic mobilization from arsenopyrite in the sodium nitrate system as compared to sodium chloride (Figure 1). With increased reaction time, iron(III) (hydr)oxide undergoes aging processes to form maghemite in the sodium nitrate system and a mixture of maghemite and hematite in the sodium chloride system. Hematite, due to its increased crystallinity, has less sorption capacity for arsenic than maghemite.<sup>62</sup> However, it is important to note that the transformation of iron(III) (hydr)oxides into more stable iron(III) oxide polymorphs can lead to the irreversible sorption of associated arsenic anions. Therefore, although these systems will have less capacity for arsenic sorption, the arsenic attenuated by the iron(III) (hydr)oxides in early stages will become strongly bound within the iron(III) oxide matrix.<sup>63</sup> This inferred trapping mechanism can be beneficial for the long-term fate and transport of arsenic in oxic or hypoxic groundwater systems where ferric iron minerals are stable.

**Inhibited Secondary Mineral Precipitation in the Wastewater System.** Another interesting new observation is the lack of precipitation in the system containing wastewater in comparison to both the sodium nitrate and sodium chloride systems. Currently, there are no studies which have reported on this apparent inhibition of iron(III) (hydr)oxide precipitation. Nonetheless, studies which model arsenic mobilization during

MAR operations have assumed the formation of ferrihydrite as an attenuation mechanism during arsenic transport in MAR.<sup>18</sup> However, this modeling study did not utilize reclaimed water as the secondary water source.

We examined this aspect further for our system by monitoring the reduction–oxidation potential (ORP) and pH over the 7-day reaction period for the wastewater, sodium nitrate, and sodium chloride aqueous solutions. ORP is a measure of the tendency of the solution to gain or lose electrons. A positive redox potential indicates oxidizing conditions, meaning that the aqueous solution is more likely to gain electrons from arsenopyrite, thereby becoming reduced while arsenopyrite is oxidized. Evolution trends in pH and ORP for aerobic reactors can be found in Figure 4.

For the 10 mM sodium nitrate and sodium chloride systems, similar evolutions were observed for pH and ORP measurements. pH decreased steadily over the 7-day period. This is likely due to the continuous oxidative dissolution of arsenopyrite through reaction eq 1a, which produces arsenous acid. For the wastewater system, the pH increased initially from 7.0 to 8.4, before decreasing again to around 7. The wastewater has a higher alkalinity than our model systems, which results in a high buffering capability. This may prevent decreases in pH observed in the nitrate and chloride systems. At a lower pH, increased arsenic mobilization would occur due to proton-promoted dissolution; however lower pH will also favor arsenic sorption onto iron(III) (hydr)oxides. Higher iron concentrations would result in higher saturation indices with regards to iron(III) (hydr)oxide precipitates. However, the higher pH in the wastewater should also contribute to higher saturation indices due to the increased hydroxide ion concentration (reaction eq 2). Because water chemistry effects on iron(III) (hydr)oxide saturation indices are contradictory, additional factors may be contributing to the inhibited precipitation for wastewater.

The ORP values provide further insight into precipitation trends. The ORP increased over the 7-day period and was generally positive for the sodium nitrate and sodium chloride systems. In contrast, the ORP in the wastewater system fluctuated but always remained negative over the reaction period. The formation of iron(III) (hydr)oxides is contingent on the oxidation of Fe(II), released through reaction eq 1a, to Fe(III). The negative redox potential in the wastewater system indicates that the condition is a reducing environment for arsenopyrite. This could prevent the oxidation of Fe(II) and precipitation of iron(III) (hydr)oxides, a process consistent with our AFM and Raman experimental observations.

The lower ORP conditions in the wastewater system are prevalent in reclaimed wastewater for reuse. In secondary wastewater treatment, low ORP conditions are necessary to facilitate biological denitrification and phosphorus removal processes.<sup>64</sup> These redox reactions are further promoted by the addition of dissolved organic carbon (DOC) serving as the electron donor. Although much of the DOC present in wastewater is removed prior to effluent discharge and reuse, the DOC levels can still be elevated when compared to groundwater concentrations.<sup>65</sup> In this study, wastewater samples had a nonpurgeable DOC concentration of 12.42 mg/L, while concentrations in the two model systems were negligible. This factor may be the root of observed differences in precipitation, as the presence of DOC would prevent the oxidation of Fe(II) and could also passivate the arsenopyrite surface, preventing heterogeneous iron(III) (hydr)oxide

precipitation. However, uncertainty exists making it necessary to quantify the effects of DOC on both arsenic mobilization from arsenopyrite and its correlation with heterogeneous and homogeneous iron(III) (hydr)oxide nucleation and growth. Therefore, although it is not in the scope of the current study, a better understanding of the effects of DOC on arsenic mobilization and secondary mineral precipitation during arsenopyrite oxidative dissolution can be a future research direction. Bicarbonate effects were also tested but could not account for observed trends in arsenic mobilization for the wastewater system. Information on bicarbonate tests can be found in SI Section S4.

**Environmental Implications.** The redox cycling of iron in the Earth's subsurface regulates the fate and transport of many elements of concern. Engineered processes such as MAR can have a drastic effect on the redox potential of groundwater environments, triggering the oxidative dissolution of reduced iron minerals including arsenopyrite. Ferric ions released from these minerals will form iron(III) (hydr)oxide minerals, attenuating mobilized arsenic. This work showed that the presence of high concentrations of chloride ions will inhibit the continued nucleation of iron(III) (hydr)oxides. In addition, the promotion of Ostwald ripening could lead to the faster phase transformation of iron(III) (hydr)oxides. As a result, the arsenic mobility is higher in systems which contain sodium chloride rather than sodium nitrate. Sites implementing MAR should therefore carefully monitor chloride concentrations in injected reclaimed water. To fully benefit from the effects of arsenic sorption onto nanoscale iron(III) (hydr)oxide precipitation, pretreatment should be utilized to minimize chloride concentrations. However, it is also important to note that the transformation of iron(III) (hydr)oxides into more stable iron(III) oxide polymorphs can lead to the irreversible sorption of associated arsenic anions, which can be beneficial for better sequestration of arsenic in oxic or hypoxic groundwater systems. Lastly, it was determined that the presence of wastewater inhibits iron(III) (hydr)oxide precipitation and decreased the ORP for this system, potentially due to the presence of DOC. Therefore, DOC is also a factor which may need to be monitored at MAR sites and controlled in order to promote iron(III) (hydr)oxide precipitation.

These observations have significant environmental implications for the longer term fate and transport of arsenic in groundwater aquifers; arsenic associated with these stable iron oxide minerals will be trapped as long as the aqueous environment is favorable for Fe(III) (e.g., oxidative environments). Activation energies for arsenic mobilization in aerobic and anaerobic systems containing sodium nitrate, sodium chloride, and wastewater samples were experimentally determined. Differences in activation energies among the systems indicate that the mechanisms controlling arsenopyrite dissolution and the propensity for arsenic mobilization can vary with dissolved oxygen presence and can therefore be useful for determining MAR operating conditions which can limit arsenic release from arsenic containing pyrite minerals. Lastly, results can be used as a basis for developing more complex model MAR systems on the laboratory scale. This basis will allow us to better interpret how future changes to the aqueous phase (e.g., addition of DOC, bicarbonate anions, and aqueous metals in Table 1) and solid phase (e.g., utilization of arsenopyrite-soil mixtures, field site samples, and arsenian pyrite (< 0.5–10 wt % As)<sup>17</sup>), are impacting the mechanisms of arsenopyrite oxidation and secondary mineral precipitation during MAR.

## ASSOCIATED CONTENT

### S Supporting Information

Detailed information on the experimental setup and additional testing related to this study. This information is available free of charge via the Internet at <http://pubs.acs.org>.

## AUTHOR INFORMATION

### Corresponding Author

\*E-mail: ysjun@seas.wustl.edu <http://encl.engineering.wustl.edu/>.

### Notes

The authors declare no competing financial interest.

## ACKNOWLEDGMENTS

We are grateful for support received from Washington University's Faculty Startup. We thank the Environmental NanoChemistry Group members for valuable discussion. C.W.N. acknowledges the generous support of the Mr. and Mrs. Spencer T. Olin Fellowship. This study was partially supported by the EPA Water Resources Adaptation Program (WRAP) research conducted with partial sponsorship under EPA Contract EP-C-09-041. The research described herein has been subjected to the Agency's administrative review and has been approved for external publication. Any opinions expressed in this paper are those of the authors and do not necessarily reflect the views of the Agency; therefore, no official endorsement should be inferred.

## REFERENCES

- (1) Bouwer, H. Integrated water management: Emerging issues and challenges. *Agric. Water Manage.* **2000**, *45* (3), 217–228.
- (2) Amelung, F.; Galloway, D. L.; Bell, J. W.; Zebker, H. A.; Lacznak, R. J. Sensing the ups and downs of Las Vegas: InSAR reveals structural control of land subsidence and aquifer-system deformation. *Geology* **1999**, *27* (6), 483–486.
- (3) Sophocleous, M. Environmental implications of intensive groundwater use with special regard to streams and wetlands. In *Intensive Use of Groundwater: Challenges and Opportunities*; Swets & Zeitlinger BV: Lisse, The Netherlands, 2003; pp 93–112.
- (4) Zektser, S.; Loaiciga, H.; Wolf, J. Environmental impacts of groundwater overdraft: Selected case studies in the southwestern United States. *Environ. Geol.* **2005**, *47* (3), 396–404.
- (5) Dillon, P. Future management of aquifer recharge. *HydJ* **2005**, *13* (1), 313–316.
- (6) Hollander, H.; Mull, R.; Panda, S. A concept for managed aquifer recharge using ASR-wells for sustainable use of groundwater resources in an alluvial coastal aquifer in Eastern India. *Phys. Chem. Earth* **2009**, *34* (4), 270–278.
- (7) Khan, S.; Mushtaq, S.; Hanjra, M. A.; Schaeffer, J. r. Estimating potential costs and gains from an aquifer storage and recovery program in Australia. *Agric. Water Manage.* **2008**, *95* (4), 477–488.
- (8) Pavelic, P.; Nicholson, B. C.; Dillon, P. J.; Barry, K. E. Fate of disinfection by-products in groundwater during aquifer storage and recovery with reclaimed water. *J. Contam. Hydrol.* **2005**, *77* (4), 351–373.
- (9) Sheng, Z. An aquifer storage and recovery system with reclaimed wastewater to preserve native groundwater resources in El Paso, Texas. *J. Environ. Manage.* **2005**, *75* (4), 367–377.
- (10) Vanderzalm, J.; Le Gal La Salle, C.; Dillon, P. Fate of organic matter during aquifer storage and recovery (ASR) of reclaimed water in a carbonate aquifer. *Appl. Geochem.* **2006**, *21* (7), 1204–1215.
- (11) Wilson, L.; Amy, G.; Gerba, C.; Gordon, H.; Johnson, B.; Miller, J. Water quality changes during soil aquifer treatment of tertiary effluent. *Water Environ. Res* **1995**, 371–376.

- (12) Asano, T.; Cotruvo, J. A. Groundwater recharge with reclaimed municipal wastewater: Health and regulatory considerations. *Water Res.* **2004**, *38* (8), 1941–1951.
- (13) Jones, G. W.; Pichler, T. Relationship between pyrite stability and arsenic mobility during aquifer storage and recovery in Southwest Central Florida. *Environ. Sci. Technol.* **2007**, *41* (3), 723–730.
- (14) Neil, C. W.; Yang, Y. J.; Jun, Y.-S. Arsenic mobilization and attenuation by mineral-water interactions: Implications for managed aquifer recharge. *J. Environ. Monit.* **2012**, *14* (7), 1772–1788.
- (15) Overacre, R.; Clinton, T.; Pyne, D.; Snyder, S.; Dillon, P. Reclaimed water aquifer storage and recovery: Potential changes in water quality. *Proc. Water Environ. Fed.* **2006**, *2006* (12), 1339–1360.
- (16) Price, R. E.; Pichler, T. Abundance and mineralogical association of arsenic in the Suwannee Limestone (Florida): Implications for arsenic release during water–rock interaction. *Chem. Geol.* **2006**, *228* (1), 44–56.
- (17) Meng, X.; Jing, C.; Korfiatis, G. P. In *A Review of Redox Transformation of Arsenic in Aquatic Environments*, ACS Symp. Ser. 2003; ACS Publications: Washington, DC, 2003; pp 70–83.
- (18) Wallis, I.; Prommer, H.; Simmons, C. T.; Post, V.; Stuyfzand, P. J. Evaluation of conceptual and numerical models for arsenic mobilization and attenuation during managed aquifer recharge. *Environ. Sci. Technol.* **2010**, *44* (13), 5035–5041.
- (19) Appelo, C. A. J.; Postma, D. *Geochemistry, Groundwater and Pollution*; Taylor & Francis: London, 2005.
- (20) Burkett, R. S.; Stoll, R. C. Naturally occurring arsenic in sandstone aquifer water supply wells of Northeastern Wisconsin. *Ground Water Monit. Rev.* **1999**, *19* (2), 114–121.
- (21) Utsunomiya, S.; Peters, S. C.; Blum, J. D.; Ewing, R. C. Nanoscale mineralogy of arsenic in a region of New Hampshire with elevated As-concentrations in the groundwater. *Am. Mineral.* **2003**, *88* (11–12), 1844–1852.
- (22) Nordstrom, D. K. Worldwide occurrences of arsenic in ground water. *Science* **2002**, *296* (5576), 2143–2145.
- (23) Gordalla, B. C.; Ewers, U.; Frimmel, F. H. Hydraulic fracturing: A toxicological threat for groundwater and drinking-water? *Environ. Earth Sci.* **2013**, *70* (8), 3875–3893.
- (24) Nicot, J.-P.; Scanlon, B. R. Water use for shale-gas production in Texas, U.S. *Environ. Sci. Technol.* **2012**, *46* (6), 3580–3586.
- (25) Murciego, A.; Alvarez-Ayuso, E.; Pellitero, E.; Rodriguez, M.; Garcia-Sanchez, A.; Tamayo, A.; Rubio, J.; Rubio, F.; Rubin, J. Study of arsenopyrite weathering products in mine wastes from abandoned tungsten and tin exploitations. *J. Hazard. Mater.* **2011**, *186* (1), 590–601.
- (26) Nesbitt, H.; Muir, I. Oxidation states and speciation of secondary products on pyrite and arsenopyrite reacted with mine waste waters and air. *Mineral. Petrol.* **1998**, *62* (1–2), 123–144.
- (27) Stollenwerk, K. G. Geochemical processes controlling transport of arsenic in groundwater: A review of adsorption. *Arsenic Ground Water* **2003**, *67*, 100.
- (28) Wang, S.; Mulligan, C. N. Natural attenuation processes for remediation of arsenic contaminated soils and groundwater. *J. Hazard. Mater.* **2006**, *138* (3), 459–470.
- (29) Postma, D.; Larsen, F.; Minh Hue, N. T.; Duc, M. T.; Viet, P. H.; Nhan, P. Q.; Jessen, S. r. Arsenic in groundwater of the Red River floodplain, Vietnam: Controlling geochemical processes and reactive transport modeling. *Geochim. Cosmochim. Acta* **2007**, *71* (21), 5054–5071.
- (30) Cheng, H.; Hu, Y.; Luo, J.; Xu, B.; Zhao, J. Geochemical processes controlling fate and transport of arsenic in acid mine drainage (AMD) and natural systems. *J. Hazard. Mater.* **2009**, *165* (1), 13–26.
- (31) Donahue, R.; Hendry, M. Geochemistry of arsenic in uranium mine mill tailings, Saskatchewan, Canada. *Appl. Geochem.* **2003**, *18* (11), 1733–1750.
- (32) Mkandawire, M.; Dudel, E. G. Accumulation of arsenic in *Lemna gibba* L.(duckweed) in tailing waters of two abandoned uranium mining sites in Saxony, Germany. *Sci. Total Environ.* **2005**, *336* (1), 81–89.
- (33) Chatterjee, A.; Das, D.; Mandal, B. K.; Chowdhury, T. R.; Samanta, G.; Chakraborti, D. Arsenic in ground water in six districts of West Bengal, India: The biggest arsenic calamity in the world. I: Arsenic species in drinking water and urine of the affected people. *Analyst* **1995**, *120* (3), 643–650.
- (34) Nickson, R.; McArthur, J.; Ravenscroft, P.; Burgess, W.; Ahmed, K. Mechanism of arsenic release to groundwater, Bangladesh and West Bengal. *Appl. Geochem.* **2000**, *15* (4), 403–413.
- (35) Costa, M.; Botelho do Rego, A.; Abrantes, L. Characterization of a natural and an electro-oxidized arsenopyrite: A study on electrochemical and X-ray photoelectron spectroscopy. *Int. J. Miner. Process.* **2002**, *65* (2), 83–108.
- (36) Stopar, J. D.; Lucey, P. G.; Sharma, S. K.; Misra, A. K.; Taylor, G. J.; Hubble, H. W. Raman efficiencies of natural rocks and minerals: Performance of a remote Raman system for planetary exploration at a distance of 10 meters. *Spectrochim. Acta A* **2005**, *61* (10), 2315–2323.
- (37) McGuire, M. M.; Banfield, J. F.; Hamers, R. J. Quantitative determination of elemental sulfur at the arsenopyrite surface after oxidation by ferric iron: Mechanistic implications. *Geochem. Trans.* **2001**, *2* (4), 25.
- (38) Furuya, N.; Matsuyuki, A.; Higuchi, S.; Tanaka, S. Determination of nitrate ion in waste and treated waters by laser raman spectrometry. *Water Res.* **1979**, *13* (4), 371–374.
- (39) Lund, L. J. Nitrogen balance in a pond system receiving tertiary effluent. *J. Environ. Qual.* **1999**, *28* (4), 1258–1263.
- (40) Greenway, M. The role of constructed wetlands in secondary effluent treatment and water reuse in subtropical and arid Australia. *Ecol. Eng.* **2005**, *25* (5), 501–509.
- (41) Reemtsma, T.; Gniru, R.; Jekel, M. Infiltration of combined sewer overflow and tertiary municipal wastewater: An integrated laboratory and field study on nutrients and dissolved organics. *Water Res.* **2000**, *34* (4), 1179–1186.
- (42) Ficklin, W. H. Separation of arsenic (III) and arsenic (V) in ground waters by ion-exchange. *Talanta* **1983**, *30* (5), 371–373.
- (43) Modesto Lopez, L. B.; Pasteris, J. D.; Biswas, P. Sensitivity of micro-Raman spectrum to crystallite size of electrospray-deposited and post-annealed films of iron-oxide nanoparticle suspensions. *Appl. Spectrosc.* **2009**, *63* (6), 627–635.
- (44) McKibben, M.; Tallant, B.; Del Angel, J. Kinetics of inorganic arsenopyrite oxidation in acidic aqueous solutions. *Appl. Geochem.* **2008**, *23* (2), 121–135.
- (45) Rau, I.; Gonzalo, A.; Valiente, M. Arsenic(V) adsorption by immobilized iron mediation. Modeling of the adsorption process and influence of interfering anions. *React. Funct. Polym.* **2003**, *54* (1–3), 85–94.
- (46) Youngran, J.; FAN, M.; Van Leeuwen, J.; Belczyk, J. F. Effect of competing solutes on arsenic (V) adsorption using iron and aluminum oxides. *JEnvS* **2007**, *19* (8), 910–919.
- (47) Guo, X.; Chen, F. Removal of arsenic by bead cellulose loaded with iron oxyhydroxide from groundwater. *Environ. Sci. Technol.* **2005**, *39* (17), 6808–6818.
- (48) Ottley, C.; Davison, W.; Edmunds, W. Chemical catalysis of nitrate reduction by iron (II). *Geochim. Cosmochim. Acta* **1997**, *61* (9), 1819–1828.
- (49) Postma, D.; Boesen, C.; Kristiansen, H.; Larsen, F. Nitrate reduction in an unconfined sandy aquifer: Water chemistry, reduction processes, and geochemical modeling. *Water Resour. Res.* **1991**, *27* (8), 2027–2045.
- (50) Sorensen, J.; Thorling, L. Stimulation by lepidocrocite ( $\gamma$ -FeOOH) of Fe (II)-dependent nitrite reduction. *Geochim. Cosmochim. Acta* **1991**, *55* (5), 1289–1294.
- (51) Yu, Y.; Zhu, Y.; Gao, Z.; Gammons, C. H.; Li, D. Rates of arsenopyrite oxidation by oxygen and Fe (III) at pH 1.8–12.6 and 15–45 °C. *Environ. Sci. Technol.* **2007**, *41* (18), 6460–6464.
- (52) Erbs, J. J.; Berquo, T. S.; Reinsch, B. C.; Lowry, G. V.; Banerjee, S. K.; Penn, R. L. Reductive dissolution of arsenic-bearing ferrihydrite. *Geochim. Cosmochim. Acta* **2005**, *74* (12), 3382–3395.

- (53) Sidhu, P.; Gilkes, R.; Cornell, R.; Posner, A.; Quirk, J. Dissolution of iron oxides and oxyhydroxides in hydrochloric and perchloric acids. *Clays Clay Miner.* **1981**, *29* (6), 269–276.
- (54) Jang, J.-H.; Dempsey, B. A.; Burgos, W. D. A model-based evaluation of sorptive reactivities of hydrous ferric oxide and hematite for U (VI). *Environ. Sci. Technol.* **2007**, *41* (12), 4305–4310.
- (55) Hu, Y.; Lee, B.; Bell, C.; Jun, Y.-S. Environmentally abundant anions influence the nucleation, growth, Ostwald ripening, and aggregation of hydrous Fe(III) oxides. *Langmuir* **2012**, *28* (20), 7737–7746.
- (56) Liu, B.; Zeng, H. C. Symmetric and asymmetric Ostwald ripening in the fabrication of homogeneous core-shell semiconductors. *Small* **2005**, *1* (5), 566–571.
- (57) Dubinina, E. O.; Lakshtanov, L. Z. A kinetic model of isotopic exchange in dissolution-precipitation processes. *Geochim. Cosmochim. Acta* **1997**, *61* (11), 2265–2273.
- (58) Liu, W.; Etschmann, B.; Brugger, J.; Spiccia, L.; Foran, G.; McInnes, B. UV-Vis spectrophotometric and XAFS studies of ferric chloride complexes in hyper-saline LiCl solutions at 25–90 °C. *Chem. Geol.* **2006**, *231* (4), 326–349.
- (59) Beckmann, W. Nucleation phenomena during the crystallisation and precipitation of Abecarnil. *J. Cryst. Growth* **1999**, *198–199, Part 2* (0), 1307–1314.
- (60) Roelands, C. P. M.; Jiang, S.; Kitamura, M.; ter Horst, J. H.; Kramer, H. J. M.; Jansens, P. J. Antisolvent crystallization of the polymorphs of l-histidine as a function of supersaturation ratio and of solvent composition. *Cryst. Growth Des.* **2006**, *6* (4), 955–963.
- (61) Dixit, S.; Hering, J. G. Comparison of arsenic(V) and arsenic(III) sorption onto iron oxide minerals: Implications for arsenic mobility. *Environ. Sci. Technol.* **2003**, *37* (18), 4182–4189.
- (62) Park, H.; Myung, N. V.; Jung, H.; Choi, H. As (V) remediation using electrochemically synthesized maghemite nanoparticles. *J. Nanopart. Res.* **2009**, *11* (8), 1981–1989.
- (63) Pedersen, H. D.; Postma, D.; Jakobsen, R. Release of arsenic associated with the reduction and transformation of iron oxides. *Geochim. Cosmochim. Acta* **2006**, *70* (16), 4116–4129.
- (64) Ra, C. S.; Lo, K. V.; Shin, J. S.; Oh, J. S.; Hong, B. J. Biological nutrient removal with an internal organic carbon source in piggery wastewater treatment. *Water Res.* **2000**, *34* (3), 965–973.
- (65) Foster, S. S.; Garduno, H.; Tuinhof, A.; Kemper, K.; Nanni, M. Urban wastewater as groundwater recharge: Evaluating and managing the risks and benefits. In *GW-MATE Briefing Note Series*, No. 12; World Bank: Washington, DC, 2003.